Weibel-like instability in magnetohydrodynamics

J. R. Davies[a)]

Laboratory for Laser Energetics, University of Rochester, Rochester, New York 14623-1299, USA

(Dated: 28 November 2023)

In magnetohydrodynamics (MHD), a density perturbation perpendicular to an electron temperature gradient generates a magnetic field around itself that acts to increase the perturbation, which can lead to instability. An MHD dispersion relation is obtained for perturbations perpendicular to a fixed electron temperature gradient with an initial in-plane magnetic field, including resistivity, viscosity, and the electrothermal coefficient. Instability occurs for sufficiently small electron temperature-gradient scale lengths determined by the ion collisionless skin depth. Both viscosity and resistivity are required to prevent growth at arbitrarily small spatial scales and to give a physical result for the fastest growing mode. The perpendicular electrothermal coefficient is only significant for a narrow range of low electron Hall parameters, causing a modest reduction in magnetic field growth and modifying the criteria for instability in the presence of viscosity. If the definition of the Weibel instability [E. S. Weibel, Phys. Rev. Lett. **2**, 83 (1959)] is extended to include all instabilities due to anisotropy in the electron velocity distribution, then this is a Weibel-like instability because an electron temperature gradient implies an anisotropic electron velocity distribution. The implications for the formation of filaments in laser-produced plasmas and for the verification of MHD codes are considered.

[a)]jdav@lle.rochester.edu

I. INTRODUCTION

In Ref. [1] we presented magnetohydrodynamic (MHD) simulations of plasma produced by a laser–solid interaction that showed the formation of filaments in the density and magnetic field, but not the temperature. The filaments observed in the simulation were in qualitative agreement with experimental data presented and many other published experimental results, which we reviewed. The formation of filaments in laser-produced plasmas continues to attract interest.[2,3] The filaments in our MHD simulations had a width determined by the grid spacing, indicative of a numerical origin. To resolve this issue, we derived a dispersion relation for density perturbations perpendicular to both an electron temperature gradient and an existing magnetic field. The dispersion relation showed that perturbations would grow at a rate that increased with wavenumber, demonstrating that the filaments were inherent to the equations of MHD, not a numerical artifact. The origin of the instability is the self-generated magnetic field proportional to $\nabla n_\mathrm{e} \times \nabla T_\mathrm{e}$, where n_e is electron density and T_e is electron temperature. A density perturbation perpendicular to an electron temperature gradient generates a magnetic field around itself, and the gradient of the magnetic pressure acts to increase the perturbation.

Growth at arbitrarily large wavenumbers is nonphysical. The equations of MHD considered lacked the physics necessary to prevent growth at arbitrarily small spatial scales. A two-fluid model, including electron dynamics, would prevent growth at spatial scales less than the electron Debye length. Here, we consider an addition to the equations of MHD that should also inhibit growth at small spatial scales: viscosity. We also include advection of the imposed magnetic field that was omitted in our original derivation,[1] which leads to stabilization for sufficiently large magnetic fields. Given the recent interest in extended MHD, we also consider the inclusion of the full magnetized transport coefficients and find that the perpendicular electrothermal coefficient leads to additional terms that could provide a means of testing its implementation in MHD codes.

There are a number of other MHD instabilities driven by an electron temperature gradient, but none that include density perturbations, only magnetic field and, in most cases, temperature perturbations, although in practice such perturbations could lead to density perturbations. The only other instability that starts with an existing magnetic field perpendicular to the temperature gradient is the field compressing magnetothermal instability,[4]

which gives growing temperature perturbations driven by cross-field heat flow and the Nernst effect. The magnetothermal instability[2] gives growing temperature perturbations driven by cross-field heat flow for initially parallel density and temperature gradients. The magnetized heat-flow-driven instability[5] gives growing, circularly polarized transverse waves driven by the perpendicular electrothermal coefficient for an existing magnetic field parallel to the temperature gradient.

Kinetic and two-fluid models considering only magnetic field perturbations also show instability driven by an electron temperature gradient perpendicular to an existing magnetic field, which is referred to as the tearing mode or self-filamentation for a uniform magnetic field.[6] In the two-fluid model, the instability is driven by a time-dependent parallel electrothermal coefficient.

Another member of the family of gradient-driven MHD instabilities that has been considered in the context of laser-plasmas is the interchange instability,[7] which gives growing magnetic field perturbations driven by a pressure gradient perpendicular to a curved magnetic field.

There are also a number of kinetic instabilities that can form filaments. The most widely mentioned instability in the context of filaments in laser-plasmas is the Weibel instability,[8] which is why we chose to use the term Weibel-like. Weibel specifically considered an electron distribution with different non-relativistic Maxwellian distributions in different directions, showing that this can be unstable in an electromagnetic, kinetic model with fixed ions. However, Weibel's key point was that anisotropy of the electron velocity distribution can lead to growing transverse waves. The definition of the Weibel instability is commonly extended to include counter streaming populations.[9,10] If we extend Weibel's definition to include longitudinal waves, then our instability is Weibel-like because an electron temperature gradient implies an anisotropic electron velocity distribution (the distribution becomes broader along one specific direction). However, there is no clear consensus on the use of the term Weibel. The term filamentation may also be used, and is certainly more descriptive. Bret, Firpo and Deutsch[10] classify beam-plasma instabilities as Weibel, filamentation, or two-stream based on the direction of the wave vector with respect to the beam and the electric field, defining Weibel as having a wave vector parallel to the beam and perpendicular to the electric field. If we use the temperature gradient to define our preferred (beam) direction, then we are considering wave vectors perpendicular to the preferred direction, which is not Weibel in the

Bret, Firpo and Deutsch classification. In a fluid model, the electron distribution assumed by Weibel would lead to anisotropy in the electron pressure tensor. The instability we are considering originates from anisotropy of the scalar electron pressure, so from this point of view could be considered Weibel-like. The key difference between our case and other Weibel-like or filamentation instabilities is that for an initially unmagnetized plasma ours is a nonlinear process. We include an initial magnetic field to allow a linear treatment, but in many practical cases we are interested in the nonlinear process.

Particle-in-cell (PIC) simulations have shown that the expansion of a uniform, cylindrical plasma[11] and of a plasma blob initiated with perpendicular electron temperature and density gradients[12] can lead to anisotropic electron velocity distributions, and hence to Weibel-like instabilities. However, PIC simulations including collisions have shown that such instability in an expanding plasma can be suppressed.[13] Another mechanism for the generation of anisotropic electron velocity distributions in laser-plasmas that has been observed in PIC simulations is Raman scattering.[14]

Laser filamentation and the radiative cooling instability are additional candidates for the formation of filaments in laser-plasmas, which we have discussed previously.[1]

The rest of this article is organized as follows: Section II outlines the derivation of the full 1-D dispersion relation. Section II A considers the values of the electrothermal coefficients appearing in the dispersion relation. The nature of solutions to specific cases are then considered. Section II B gives the full solution for ideal MHD (no resistivity, no electrothermal coefficient, no viscosity). Section II C considers the growth criterion and the fastest growing mode for resistive MHD (no viscosity). Section II D considers the growth criteria in the presence of both resistivity and viscosity. Section III briefly considers the 2-D case of perturbations at an angle to the initial magnetic field but perpendicular to the temperature gradient, outlining the derivation and considering the fastest growing mode for resistive MHD. Some applications of the theory are then discussed. Section IV considers the formation of filaments in laser-produced plasmas, using the derived dispersion relation to estimate growth rates and growing wavelengths. Section V considers the application of the results to MHD codes, in particular, testing the implementation of self-generated magnetic field and the perpendicular electrothermal coefficient. Finally, Sec. VI summarizes our key conclusions.

II. ONE-DIMENSIONAL DISPERSION RELATION

We are interested in understanding the evolution of density perturbations perpendicular to an electron temperature gradient by obtaining a dispersion relation from linearized MHD equations, which requires us to consider a somewhat artificial and not entirely self-consistent set of steady-state initial conditions. Therefore, we must consider the results as only indicative of what could occur in experiments and simulations. It is perfectly possible, however, to implement such conditions in an MHD code, making our result a useful test problem for such codes.

First, we impose a fixed electron temperature gradient in one direction, T'_{e} (eV m^{-1}), which we define to be the x direction, and ignore dynamics in this direction. In practice, we would require a heat source in equilibrium with thermal transport to maintain the temperature gradient, which is not an unreasonable assumption for many cases of interest. A situation with no advection of either density or magnetic field along the direction of the temperature gradient is not possible in practice, so we must assume that the changes caused by such advection in the plane of interest are slow compared to the growth rates we obtain. Including dynamics in the direction of the temperature gradient leads to a multidimensional problem with no steady-state solution that is not amenable to simple, analytic models.

Magnetic pressure is proportional to the square of the magnetic field, which means that it will only be present in a linear model if there is an initial magnetic field. We will therefore assume a uniform initial magnetic field B_0, perpendicular to the temperature gradient, which we use to define the y direction.

To give a 1-D result we will consider dynamics only perpendicular to both the temperature gradient and the initial magnetic field, which is the z direction. To further simplify the equations, we will assume that there is no steady-state velocity. We can write our MHD variables as

$$\nabla T_{\mathrm{e}} = T'_{\mathrm{e}}\hat{x} \tag{1}$$

$$\vec{B} = B_0[1 + B_1(z,t)]\hat{y} \tag{2}$$

$$\rho = \rho_0[1 + \rho_1(z,t)], \tag{3}$$

$$\vec{v} = v_1(z,t)\hat{z}, \tag{4}$$

where T_e is electron temperature in eV; B is magnetic field (T); ρ is mass density (kg m^{-3}); v is fluid velocity (m s^{-1}); subscript 0 indicates initial, steady-state values; subscript 1 indicates the perturbations (we use dimensionless forms for B_1 and ρ_1 expressed as fractions of the initial values); and the hats indicate unit vectors. Note that T_e' and B_0 are positive due to the definition of the axes.

Linearizing the continuity equation, the momentum equation, and Faraday's law in the perturbed variables gives

$$\frac{\partial \rho_1}{\partial t} = -\frac{\partial v_1}{\partial z}, \tag{5}$$

$$\frac{\partial v_1}{\partial t} = -\frac{\partial}{\partial z}\frac{p_{e1} + p_{i1}}{\rho_0} - v_A^2 \frac{\partial B_1}{\partial z} + D_v \frac{\partial^2 v_1}{\partial z^2}, \tag{6}$$

$$\frac{\partial B_1}{\partial t} = -\frac{\partial v_1}{\partial z} + \frac{\partial \beta_\perp}{\partial z}\frac{T_e'}{B_0} + D_B \frac{\partial^2 B_1}{\partial z^2} - \frac{\partial \rho_1}{\partial z}\frac{T_e'}{B_0}, \tag{7}$$

where p is pressure (Pa), we have introduced the Alfvén velocity,

$$v_A^2 = \frac{B_0^2}{\mu_0 \rho_0}, \tag{8}$$

where μ_0 is permeability of free space ($4\pi \times 10^{-7}$ H m^{-1}), diffusion coefficients (m^2 s^{-1}) for velocity and magnetic field given by

$$D_v = \frac{4}{3}\nu_0, \; D_B = \frac{\eta_{\perp 0}}{\mu_0}, \tag{9}$$

where ν is kinematic viscosity (m^2 s^{-1}) and $\eta_\perp$ is perpendicular resistivity (Ω m), and the perpendicular electrothermal coefficient $\beta_\perp$ (dimensionless). To first order, no terms have been neglected. Our previous treatment[1] did not include the last term in Eq. (6) and the first two terms on the right-hand side of Eq. (7).

To close the set of equations, we assumed isothermal conditions with equal electron and ion temperatures in our previous derivation, based on the absence of small-scale temperature perturbations in the MHD simulations, a result of thermal conduction. To give a more general result we will use separate adiabatic relations for the ions and the electrons,

$$p\rho^{-\gamma} = p_0 \rho_0^{-\gamma}. \tag{10}$$

Isothermal conditions are obtained by using an adiabatic index γ of one.

We need to express $\partial\beta_\perp/\partial z$ in Eq. (7) in terms of the perturbed variables. The perpendicular electrothermal coefficient for a given atomic number Z is a function of only the electron Hall parameter

$$\chi_\mathrm{e} = 3\sqrt{\frac{\pi}{2}}\frac{4\pi\varepsilon_0^2 T_\mathrm{e}^{3/2} B}{Z^2 e^{3/2}\sqrt{m_\mathrm{e}} n_\mathrm{i} \ln\Lambda}, \tag{11}$$

where T_e is in eV, ε_0 is the permittivity of free space (8.85×10^{-12} F m^{-1}), m_e is electron mass (9.11×10^{-31} kg), e is electron charge (1.60×10^{-19} C), n_i is ion number density (m^{-3}), and $\ln\Lambda$ is the Coulomb logarithm for electron-ion scattering. The Hall parameter is dimensionless and can be expressed in terms of a ratio of mean free path to Larmor radius or cyclotron period to collision time. Using $p_\mathrm{e} \propto \rho T_\mathrm{e}$ (ideal gas) and Eq. (10), we can write

$$\frac{\partial\beta_\perp(\chi_\mathrm{e})}{\partial z} = \chi_{\mathrm{e}0}\frac{\mathrm{d}\beta_{\perp 0}}{\mathrm{d}\chi_{\mathrm{e}0}}\left[\frac{\partial B_1}{\partial z} + \left(\frac{3}{2}\gamma_\mathrm{e} - \frac{5}{2}\right)\frac{\partial \rho_1}{\partial z}\right]. \tag{12}$$

The first term in square brackets on the right hand side of Eq. (12) has the form of an advection term for B_1, so we will write it as

$$\frac{\partial B_1}{\partial t} = -v_\beta \frac{\partial B_1}{\partial z}, \tag{13}$$

where the velocity

$$v_\beta = \frac{\chi_{\mathrm{e}0}}{B_0}\left|\frac{\mathrm{d}\beta_{\perp 0}}{\mathrm{d}\chi_{\mathrm{e}0}}\right| T_\mathrm{e}'. \tag{14}$$

Note that $\mathrm{d}\beta_\perp/\mathrm{d}\chi_\mathrm{e}$ is negative so we have introduced the absolute value to leave no doubt that v_β is positive (in the $\nabla T_\mathrm{e} \times \vec{B}_0$ direction). The second term in square brackets on the right hand side of Eq. (12) has the form of the final, source term in Eq. (7), so we add it to the source term, rewriting the source term as

$$\frac{\partial B_1}{\partial t} = -\frac{\partial \rho_1}{\partial z}\frac{T_\mathrm{e}'}{B_0} f_\beta, \tag{15}$$

where

$$f_\beta = 1 - \left(\frac{5}{2} - \frac{3}{2}\gamma_\mathrm{e}\right)\chi_{\mathrm{e}0}\left|\frac{\mathrm{d}\beta_{\perp 0}}{\mathrm{d}\chi_\mathrm{e}}\right|. \tag{16}$$

Fourier transforming Eqs. (5) – (7) in space and time, or equivalently assuming that perturbed quantities vary as $\exp[i(\omega t + kz)]$, where ω is a complex frequency (s^{-1}) and k is a

real wavenumber (m^{-1}), and then eliminating the perturbed amplitudes gives the dispersion relation

$$\omega^3 + \omega^2(v_\beta k - ik^2 D_B - ik^2 D_v) - \omega k^2(v_{\mathrm{ms}}^2 + k^2 D_B D_v + ikv_\beta D_v) \\ + ik^4 c_s^2 D_B - k^3 v_\beta c_s^2 + k^3 V^3 = 0, \tag{17}$$

where we have introduced the magnetosonic velocity,

$$v_{\mathrm{ms}}^2 = v_{\mathrm{A}}^2 + c_{\mathrm{s}}^2, \tag{18}$$

the sound speed

$$c_{\mathrm{s}}^2 = \frac{\gamma_{\mathrm{e}} p_{\mathrm{e}0} + \gamma_{\mathrm{i}} p_{\mathrm{i}0}}{\rho_0}, \tag{19}$$

and a characteristic velocity for waves driven by the temperature gradient

$$V^3 = \frac{B_0 T'}{\mu_0 \rho_0} f_\beta. \tag{20}$$

Writing the temperature gradient as T_{e}/L we can write V in terms of the Alfvén velocity, the sound speed, and a dimensionless temperature gradient scale length $\hat{L}$ given by

$$\hat{L} = \frac{L}{\delta_{\mathrm{i}}} \frac{Z\gamma_{\mathrm{e}} + \gamma_{\mathrm{i}} T_{\mathrm{i}}/T_{\mathrm{e}}}{Z}, \tag{21}$$

where δ_{i} is the ion collisionless skin depth

$$\delta_{\mathrm{i}} = \frac{c}{\omega_{\mathrm{pi}}} = \sqrt{\frac{A m_{\mathrm{p}}}{Z n_{\mathrm{e}} \mu_0 e^2}}, \tag{22}$$

where c is the speed of light (3.00×10^8 m s^{-1}), ω_{pi} is the ion plasma frequency (s^{-1}), A is ion mass number, and m_{p} is proton mass (1.67×10^{-27} kg). The resulting expression for V is

$$V^3 = \frac{v_{\mathrm{A}} c_{\mathrm{s}}^2}{\hat{L}} f_\beta, \tag{23}$$

which is a form of geometric mean of the Alfvén velocity and the ion sound speed, weighted towards the ion sound speed.

The importance of the ion collisionless skin depth for self-generated magnetic field in

MHD has been pointed out by Haines,[15] who found that the ratio of temperature gradient scale length to ion collisionless skin depth determined regimes of magnetic field saturation in a steady-state model. The ratio of the temperature gradient scale length to the ion collisionless skin depth has also been found to determine the transition from MHD-like self-generated magnetic field to kinetic Weibel dominated magnetic field generation in PIC simulations.[12,13]

Equation (17) is our central result and can be solved exactly. Unfortunately, the general solution to a cubic equation is long and uninformative, even more so when the coefficients are complex numbers, which requires the solution of two cubic equations to separate real and imaginary parts of the solutions. In the following sections we will examine a series of special cases to illustrate the physical implications of various terms in Eq. (17), but first, we will evaluate the new terms f_β and v_β from the perpendicular electrothermal coefficient.

A. Electrothermal terms

We have separated the effect of the perpendicular electrothermal coefficient into two parts for convenience; a reduction factor for the self-generated magnetic field f_β [Eq. (16)] and a magnetic field advection velocity v_β [Eq. (14)], both of which originate from cross-field advection of magnetic field (in the $\nabla T_\mathrm{e} \times \vec{B}_0$ direction).

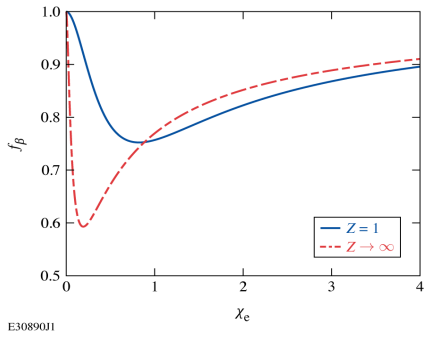

FIG. 1. Values of f_β [Eq. (16)] for isothermal electrons at $Z = 1$ and $Z \to \infty$ using the fit from Sadler, Walsh, and Li.[16]

The value of f_β depends on the electron adiabatic index γ_e [Eq. (10)]. For $\gamma_\mathrm{e} = 5/3$, which corresponds to adiabatic, nonrelativistic, nondegenerate electrons, we have $f_\beta = 1$, so the

perpendicular electrothermal coefficient has no effect on the self-generated magnetic field. Isothermal electrons ($\gamma_e = 1$) are a more reasonable approximation since thermal conduction will smooth temperature perturbations at the large wavenumbers of interest,[1] which gives the smallest possible value of f_β since $\gamma_e < 1$ is not a physically relevant value. Figure 1 shows f_β for isothermal electrons at $Z = 1$ and $Z \to \infty$ using the fit from Sadler, Walsh, and Li.[16] We note that Braginskii's fit[17] gives the incorrect limiting form for $\chi_e \to \infty$, and that the fits of Epperlein–Haines[18] and Ji–Held[19] give incorrect limiting forms for $\chi_e \to 0$. The smallest possible value of f_β is 0.59 at $\chi_e = 0.19$ for $Z \to \infty$; for $Z = 1$, the smallest value is 0.75 at $\chi_e = 0.82$. Therefore, the effect of the perpendicular electrothermal coefficient on the self-generated magnetic field can be neglected for most purposes.

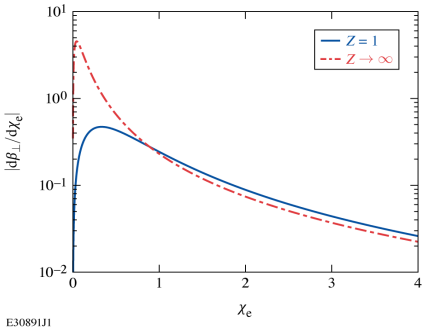

FIG. 2. Values of $|\mathrm{d}\beta_\perp/\mathrm{d}\chi_e|$ at $Z = 1$ and $Z \to \infty$ using the fit from Sadler, Walsh, and Li.[16]

To estimate the relative magnitude of v_β we compare it to the sound speed for an isothermal, ideal gas with equal electron and ion temperatures,

$$\frac{v_\beta}{c_s} = \frac{\lambda_{ei}}{L}\sqrt{\frac{A}{Z+1}}\sqrt{\frac{m_p}{m_e}}\left|\frac{\mathrm{d}\beta_\perp}{\mathrm{d}\chi_e}\right|, \tag{24}$$

where λ_{ei} is the mean free path for electron-ion scattering,

$$\lambda_{ei} = 3\sqrt{\frac{\pi}{2}}\frac{4\pi\varepsilon_0^2 T_e^2}{Z^2 e^2 n_i \ln\Lambda}, \tag{25}$$

where T_e is in eV. Figure 2 shows $|d\beta_\perp/d\chi_e|$ for $Z = 1$ and $Z \to \infty$ using the fit from Sadler, Walsh and Li.[16] The function sharply peaks at small values of χ_e, falls as $\chi_e^{-8/3}$ for large values, and increases with Z. The derivative of Sadler, Walsh, and Li's fit gives a very long

expression, so for convenience we provide a simple fit for the maximum value

$$\left|\frac{\mathrm{d}\beta_\perp}{\mathrm{d}\chi_\mathrm{e}}\right|_\mathrm{max} = 4.546\frac{Z-0.2235}{Z+6.575}, \tag{26}$$

and the value of χ_e where the maximum occurs

$$\chi_\mathrm{max} = 0.04357\frac{Z+7.437}{Z+0.1068}. \tag{27}$$

It appears that the value of v_β near the value of χ_e given by Eq. (27) could greatly exceed any other characteristic velocity of MHD, particularly at high Z, because it is naturally expressed in terms of the electron thermal velocity. The term λ_ei/L, however, is assumed to be much less than one in the derivation of the transport coefficients,[16–19] and kinetic effects result in its effective value always being less than one. Crudely speaking, one can consider kinetic effects to limit the smallest effective value of L to be the appropriate electron mean free path for the transport process under consideration.[20] In the context of thermal transport, this leads to the familiar flux limiting. Using results from kinetic calculations for thermal conduction[20] gives

$$\frac{v_{\beta\,\mathrm{max}}}{c_\mathrm{s}} \sim a0.16\frac{Z-0.2235}{Z+6.575}\sqrt{\frac{Z+4.2}{(Z+1)(Z+0.24)}}\sqrt{\frac{A}{Z}}\sqrt{\frac{m_\mathrm{p}}{m_\mathrm{e}}}, \tag{28}$$

where the constant a varies from 1 to 1.89, depending on the precise details of the kinetic calculations used. Magnetization of the electrons reduces the effective mean free path at high electron Hall parameters [Eq. (11)], but at high electron Hall parameters the gradient of the electrothermal coefficient falls as $\chi_\mathrm{e}^{-8/3}$, so Eq. (28) should remain an adequate estimate for the maximum value of v_β.

Equation (28) is weakly dependent on Z for values of interest, giving $a1.5\sqrt{A/2}$ at $Z = 1$, peaking at roughly $a1.7\sqrt{A/(Z+1)}$ for $Z = 2$ to 5, and only falling to $a0.89\sqrt{A/(Z+1)}$ at $Z = 50$. The maximum possible value of v_β/c_s in this approximation is roughly 5. However, the effective mean free path for the perpendicular electrothermal coefficient should differ from that for thermal conduction,[20] so kinetic calculations will be required to give an accurate result for the maximum value of v_β, which are beyond the scope of this work.

Overall, we can conclude that v_β will only be significant compared to other characteristic

velocities of MHD for a narrow range of small values of the electron Hall parameter close to that given by Eq. (27).

B. Ideal MHD

In ideal MHD, Eq. (17) reduces to a depressed cubic with real coefficients, making it the simplest possible case. The ideal MHD solution is also the limiting solution for small wavenumbers $k \ll (D_B + D_v)/V$ in the absence of the electrothermal term, which should be valid for $v_\beta \ll V$.

Growth occurs when,

$$V > \frac{2^{1/3}}{\sqrt{3}} v_{\rm ms}. \tag{29}$$

Writing V in terms of $v_{\rm A}$, $c_{\rm s}$ and $\hat{L}$ [Eq. (23)] we can obtain

$$\hat{L} < \frac{3^{3/2}}{2} \frac{v_{\rm A}/c_{\rm s}}{(1 + v_{\rm A}^2/c_{\rm s}^2)^{3/2}}. \tag{30}$$

The right-hand side of Eq. (30) has a maximum value of 1 when $v_{\rm A}/c_{\rm s}$ equals $1/\sqrt{2}$; therefore, growth can only occur in ideal MHD below a maximum value of $\hat{L}$:

$$\hat{L}_{\rm max} = 1. \tag{31}$$

Below $\hat{L}_{\rm max}$ there will be minimum and maximum values of $v_{\rm A}/c_{\rm s}$ for growth, but the solution of the cubic Eq. (30) does not give straightforward expressions for these limits. Furthermore, we will see that the minimum and maximum values of $v_{\rm A}/c_{\rm s}$ are significantly modified by any nonzero resistivity and viscosity.

To write the full solution to the ideal MHD dispersion relation in a compact form, we introduce the variables

$$s_\pm = \frac{Vk}{2^{1/3}} \left(-1 \pm \sqrt{1 - \frac{4 v_{\rm ms}^6}{27 V^6}} \right)^{1/3}, \tag{32}$$

where any one of the three cube roots may be used. The three solutions can then be written

as

$$\omega_1 = s_+ + s_-, \tag{33}$$

$$\omega_{2,3} = -\frac{s_+ + s_-}{2} \pm i\frac{\sqrt{3}}{2}(s_+ - s_-). \tag{34}$$

The solution to even this simple cubic equation provides us with no immediate physical insights. To understand the physical implications, it helps to consider the two limiting cases $V \gg v_{\rm ms}$ and $V \ll v_{\rm ms}$, using an expansion in the small velocity ratio. In the unstable limit

$$V \gg v_{\rm ms} \tag{35}$$

$$\omega_1 \approx -Vk\left(1 + \frac{v_{\rm ms}^2}{3V^2}\right), \tag{36}$$

$$\omega_{2,3} = \frac{Vk}{2}\left(1 + \frac{v_{\rm ms}^2}{3V^2}\right) \pm i\frac{\sqrt{3}}{2}Vk\left(1 - \frac{v_{\rm ms}^2}{3V^2}\right), \tag{37}$$

where we have retained only the leading terms in $v_{\rm ms}/V$. The first solution is a wave with group and phase velocities of approximately V traveling in the $-\nabla T_{\rm e} \times \vec{B}_0$ direction, and the two following solutions are waves with velocities of approximately $V/2$ traveling in the $\nabla T_{\rm e} \times \vec{B}_0$ direction, one damped and one growing. The magnetosonic term increases the velocities and reduces the damping and growth rates. Wave propagation has a stablizing effect because the density perturbations are moved away from the pinching magnetic field growing around them. The growth rate tends to infinity as wavenumber tends to infinity, which is nonphysical and a potential issue for MHD codes. In the opposite limit

$$V \ll v_{\rm ms} \tag{38}$$

$$\omega_1 \approx v_{\rm ms}k\frac{V^3}{3^{5/6}v_{\rm ms}^3}, \tag{39}$$

$$\omega_{2,3} = v_{\rm ms}k\left(\pm 1 - \frac{1}{2}\frac{V^3}{3^{5/6}v_{\rm ms}^3}\right), \tag{40}$$

where we have retained only the leading terms in $V/v_{\rm ms}$. The first solution is a slow wave traveling in the $\nabla T_{\rm e} \times \vec{B}_0$ direction that vanishes in the absence of an electron temperature gradient, and the two following solutions are magnetoacoustic waves traveling in the $\pm\nabla T_{\rm e} \times \vec{B}_0$ directions, with the wave traveling in the $\nabla T_{\rm e} \times \vec{B}_0$ direction having a slightly lower velocity due to the electron temperature gradient.

C. Resistive MHD

We will now add resistivity and the electrothermal terms to ideal MHD. While the full solutions become unwieldy, the criterion for growth simply becomes

$$\frac{v_\mathrm{A}}{c_\mathrm{s}} < \frac{f_\beta}{\hat{L}}. \tag{41}$$

Unlike ideal MHD, there is no fixed maximum value of $\hat{L}$ and no minimum value of $v_\mathrm{A}/c_\mathrm{s}$ for growth. Equation (41) can be rewritten as an upper limit on the magnetic field

$$B < \frac{f_\beta T_\mathrm{e}}{c_\mathrm{s} L}, \tag{42}$$

which is Haines' advection-limited magnetic field[15] with an advection velocity of the sound speed, enhanced by advection due to the electrothermal coefficient (c_s/f_β). We do not obtain Haines' diffusion-limited magnetic field ($\sim T_\mathrm{e}/D_B$) because we imposed a uniform B_0 that is not subject to diffusion. We did not obtain Eqs. (41) and (42) in our previous work[1] because we did not consider advection of the magnetic field.

The maximum growth rate occurs for wavenumber tending to infinity, which gives the simple solutions

$$\omega \to \pm c_\mathrm{s} k + i \frac{f_\beta v_\mathrm{A} c_\mathrm{s}}{2 D_B \hat{L}} \left(\frac{v_\mathrm{A} \hat{L}}{f_\beta c_\mathrm{s}} \mp 1 \right), \quad k \to \infty. \tag{43}$$

The third solution vanishes in this limit. Equation (43) corresponds to acoustic waves traveling in the $\pm \nabla T_\mathrm{e} \times \vec{B}_0$ directions, with the wave traveling in the $-\nabla T_\mathrm{e} \times \vec{B}_0$ direction being damped and the wave traveling in the $\nabla T_\mathrm{e} \times \vec{B}_0$ either being damped at a slower rate or growing, depending on the criterion given by Eq. (41). The modes tend to acoustic waves in the high wavenumber limit because resistive diffusion damps the magnetic field oscillations. Growth at arbitrarily small scales is nonphysical, but the finite growth rate for $k \to \infty$ gives us a useful formula to estimate the maximum possible growth rate of the instability. The growth rate from Eq. (43) has a maximum in $v_\mathrm{A}/c_\mathrm{s}$

$$\gamma_\mathrm{max} = \frac{f_\beta^2 c_\mathrm{s}^2}{8 D_B \hat{L}^2}, \quad \frac{v_\mathrm{A}}{c_\mathrm{s}} = \frac{f_\beta}{2\hat{L}}. \tag{44}$$

Replacing $\hat{L}$ with our original MHD variables gives

$$\gamma = \frac{B_0}{2\rho_0\eta_0}\left(\frac{f_\beta T_\mathrm{e}'}{c_\mathrm{s}} - B_0\right), \tag{45}$$

$$\gamma_\mathrm{max} = \frac{f_\beta^2 T_\mathrm{e}'^2}{8\rho_0\eta_0 c_\mathrm{s}^2},\ B_0 = \frac{f_\beta T_\mathrm{e}'}{2c_\mathrm{s}}. \tag{46}$$

To damp the acoustic waves at large wavenumbers, giving a maximum wavenumber for growth, we must add viscosity.

D. Viscosity

Finally, we add viscosity to give the full dispersion relation. Adding viscosity without resistivity is not of interest because the growth rate still tends to infinity as wavenumber tends to infinity, and growth becomes possible for all values of $\hat{L}$ and $v_\mathrm{A}/c_\mathrm{s}$.

The condition for growth to occur for the full dispersion relation is cumbersome, so we will adopt normalized variables to shorten the expression, eliminating c_s and D_B since we are not interested in the limits where either of these variables go to zero,

$$\hat{\omega} = \frac{D_B}{c_\mathrm{s}^2}\omega,\ \hat{k} = \frac{\sqrt{D_B D_v}}{c_s}k,\ R = \frac{D_v}{D_B},\ \hat{v}_\mathrm{A} = \frac{v_\mathrm{A}}{c_\mathrm{s}},\ \hat{v}_\beta = \frac{R}{1+R}\frac{v_\beta}{c_\mathrm{s}}. \tag{47}$$

Note that both $\hat{k}$ and $\hat{v}_\beta$ vanish in the absence of viscosity. We can now write the condition for growth as

$$\frac{f_\beta \hat{v}_\mathrm{A}}{\hat{L}} > \left(\sqrt{\frac{1}{1+R} + \frac{\hat{v}_\beta^2}{4}} - \frac{\hat{v}_\beta}{2}\right)\left(\frac{\hat{v}_\beta}{R} + \hat{v}_\mathrm{A}^2 + \hat{k}^2 + \frac{R}{1+R}\right) + \frac{2+R}{1+R}\hat{v}_\beta. \tag{48}$$

The implications of Eq. (48) become clearer if we rearrange it. To shorten the rearranged equation we introduce

$$f = \sqrt{\frac{1}{1+R} + \frac{\hat{v}_\beta^2}{4}} - \frac{\hat{v}_\beta}{2}, \tag{49}$$

which we note is less than 1 and decreases as $\hat{v}_\beta$ and R increase. Writing

$$\left(\hat{v}_\mathrm{A} - \frac{f_\beta}{2f\hat{L}}\right)^2 + \hat{k}^2 < \frac{f_\beta^2}{4f^2\hat{L}^2} - \frac{R}{1+R} - \frac{\hat{v}_\beta}{R} - \frac{2+R}{1+R}\frac{\hat{v}_\beta}{f}, \tag{50}$$

we see that growth occurs within a circular region of $(\hat{v}_\mathrm{A}, \hat{k})$ space. The square of the radius given by the right hand side of Eq. (50) must be greater than zero for growth to occur, which gives a maximum value of $\hat{L}$. Examples of regions of growth are given in Fig. 3, illustrating how it changes with R, and how v_β reduces the region of growth if $R < 1$ and increases it if $R > 1$.

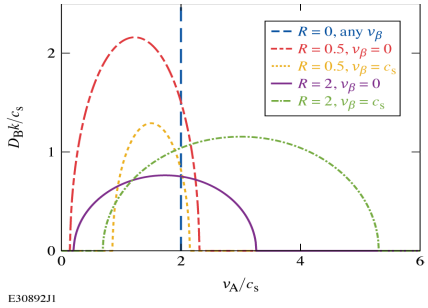

FIG. 3. Regions of growth in (v_A, k) space for $\hat{L} = f_\beta/2$ and different values of R and v_β.

Simple growth criteria are obtained in limiting cases. When the v_β terms are negligible, which requires

$$v_\beta \ll R c_\mathrm{s}, \;\; v_\beta \ll \frac{c_\mathrm{s}}{\sqrt{R}}, \tag{51}$$

we have

$$\hat{L}_\mathrm{max} \approx \frac{1+R}{2\sqrt{R}} f_\beta, \tag{52}$$

which has a minimum value of f_β when $R = 1$. Interestingly, $R = 1$ gives the same result as ideal MHD [Eq. (31)] where both viscosity and resistivity are zero, in the absence of the electrothermal coefficient. Either $R \ll 1$ or $R \gg 1$ give $\hat{L}_\mathrm{max} \gg 1$. The minimum and maximum values of v_A are given by

$$\frac{v_\mathrm{A}}{c_\mathrm{s}} \approx \sqrt{1+R}\frac{f_\beta}{2\hat{L}}\left(1 \pm \sqrt{1 - \frac{\hat{L}^2}{\hat{L}^2_\mathrm{max}}}\right). \tag{53}$$

The maximum value of v_A corresponds to a maximum magnetic field, which for $\hat{L} \ll \hat{L}_\mathrm{max}$ gives

$$B < \sqrt{1+R}\frac{f_\beta T_\mathrm{e}}{c_\mathrm{s} L}. \tag{54}$$

Compared to Eq. (42), we see that viscosity increases the maximum magnetic field, which can be attributed to an effective reduction in the advection velocity of the magnetic field. The limit on k is given by

$$k_{\max} \approx \frac{\sqrt{1+R}}{\sqrt{R}} \frac{f_\beta c_\mathrm{s}}{2\hat{L} D_B} \sqrt{1 - \frac{\hat{L}^2}{\hat{L}_{\max}^2}}. \tag{55}$$

We will now consider limits where v_β modifies the results. For

$$R \ll 1,\ v_\beta \ll \frac{c_\mathrm{s}}{R}, \tag{56}$$

the value of $\hat{L}_{\max}$ is decreased by v_β,

$$\hat{L}_{\max} \approx \frac{f_\beta}{2\sqrt{R + v_\beta/c_\mathrm{s}}}, \tag{57}$$

while Eqs. (53) and (55) remain valid, which reduces the radius of the region of growth. For

$$R \gg 1,\ v_\beta \gg \frac{c_\mathrm{s}}{\sqrt{R}}, \tag{58}$$

Eq. (52) is unchanged but the region of growth is increased by v_β,

$$\frac{v_\mathrm{A}}{c_\mathrm{s}} \approx R \frac{v_\beta}{c_\mathrm{s}} \frac{f_\beta}{2\hat{L}} \left(1 \pm \sqrt{1 - \frac{\hat{L}^2}{\hat{L}_{\max}^2}} \right), \tag{59}$$

$$k_{\max} \approx \frac{f_\beta \sqrt{R} v_\beta}{2\hat{L} D_B} \sqrt{1 - \frac{\hat{L}^2}{\hat{L}_{\max}^2}}. \tag{60}$$

The decrease in the region of growth with v_β for $R < 1$ has the potential to halt the instability as the electron Hall parameter approaches the value given by Eq. (27). The increase in the region of growth with v_β for $R > 1$ is unlikely to have any significant effect in practice because the growth in the magnetic field would rapidly reduce v_β, as seen in Fig. 2.

III. TWO-DIMENSIONAL DISPERSION RELATION

We now extend the analysis to a plane perpendicular to the fixed electron temperature gradient $T_\mathrm{e}'\hat{x}$, the (y, z) plane, where modes can be at an angle θ to the zero-order magnetic

field $B_0\hat{y}$. The 1-D dispersion relation only considered modes perpendicular to the magnetic field. The principle motivation for extending to 2-D is to provide a more general test problem for self-generated magnetic field and the perpendicular electrothermal coefficient in MHD codes; the 1-D result was already difficult to deal with analytically. To simplify what is already a very lengthy problem, we will not consider the variation in resistivity and viscosity with magnetic field, which is at most a factor of 2 perpendicular to the field. The linearized set of equations then become

$$\frac{\partial \rho_1}{\partial t} = -\frac{\partial v_{y1}}{\partial y} - \frac{\partial v_{z1}}{\partial z}, \tag{61}$$

$$\frac{\partial v_{y1}}{\partial t} = -c_\mathrm{s}^2 \frac{\partial \rho_1}{\partial y} + \frac{4}{3}\nu \frac{\partial^2 v_{y1}}{\partial y^2} + \nu \frac{\partial^2 v_{y1}}{\partial z^2} + \frac{\nu}{3}\frac{\partial^2 v_{z1}}{\partial y \partial z}, \tag{62}$$

$$\frac{\partial v_{z1}}{\partial t} = -c_\mathrm{s}^2 \frac{\partial \rho_1}{\partial z} - v_\mathrm{A}^2 \frac{\partial B_{y1}}{\partial z} + v_\mathrm{A}^2 \frac{\partial B_{z1}}{\partial y} + \frac{4}{3}\nu \frac{\partial^2 v_{z1}}{\partial z^2} + \nu \frac{\partial^2 v_{z1}}{\partial y^2} + \frac{\nu}{3}\frac{\partial^2 v_{y1}}{\partial y \partial z}, \tag{63}$$

$$\frac{\partial B_{y1}}{\partial t} = -\frac{\partial v_{z1}}{\partial z} - v_\beta \frac{\partial B_{y1}}{\partial z} + D_B \frac{\partial^2 B_{y1}}{\partial z^2} - D_B \frac{\partial^2 B_{z1}}{\partial y \partial z} - f_\beta \frac{\partial \rho_1}{\partial z}\frac{T_\mathrm{e}'}{B_0}, \tag{64}$$

$$\frac{\partial B_{z1}}{\partial z} = -\frac{\partial B_{y1}}{\partial y}. \tag{65}$$

Note that we do not need both the z component of Faraday's law and $\nabla \cdot \vec{B} = 0$ to give an equation for B_{z1}, so we chose the latter since it is simpler. The resulting 2-D dispersion relation can be written

$$\begin{aligned}\omega^4 + \omega^3 k\left(v_{\beta\theta} - iD_B k - i\frac{7}{3}\nu k\right) - \omega^2 k^2\left(v_\mathrm{ms}^2 + \frac{4}{3}\nu^2 k^2 + \frac{7}{3}D_B \nu k^2 + i\frac{7}{3}\nu v_{\beta\theta} k\right) \\ +\omega k^3\left(iv_\mathrm{ms}^2 \nu k + iv_\mathrm{A}^2 \frac{\nu}{3} k\cos^2\theta + ic_\mathrm{s}^2 D_B k + i\frac{4}{3}D_B \nu^2 k^3 - c_\mathrm{s}^2 v_{\beta\theta} - \frac{4}{3}\nu^2 v_{\beta\theta} k^2 + V_\theta^3\right) \\ +v_\mathrm{A}^2 c_\mathrm{s}^2 k^4 \cos^2\theta + c_\mathrm{s}^2 D_B \nu k^6 + ic_\mathrm{s}^2 \nu v_{\beta\theta} k^5 - iV_\theta^3 \nu k^5 = 0,\end{aligned} \tag{66}$$

where

$$v_{\beta\theta} = v_\beta \sin\theta,\ V_\theta^3 = V^3 \sin\theta. \tag{67}$$

It is not immediately obvious that the quartic Eq. (66) is equivalent to the cubic Eq. (17) when $\theta = \pi/2$; however, it is then possible to extract a factor of $w - i\nu k^2$ from Eq. (66), which gives an evanescent mode of no interest and Eq. (17) for the three remaining modes. In the opposite limit of $\theta = 0$, the terms due to the temperature gradient V_θ and $v_{\beta\theta}$ are zero; Eq. (66) can be separated into two quadratic equations, one for damped transverse or

Alfvén waves, and the other for damped longitudinal or acoustic waves. The solution for Alfvén waves is

$$\omega = \pm\sqrt{v_{\rm A}^2 - \left(\frac{D_B - \nu}{2}\right)^2 k^2}\; k + i\frac{D_B + \nu}{2}k^2. \tag{68}$$

The solution for acoustic waves is

$$\omega = \pm\sqrt{c_{\rm s}^2 - \frac{4}{9}\nu^2 k^2}\; k + i\frac{2}{3}\nu k^2, \tag{69}$$

which is the solution to the 1-D dispersion relation [Eq. (17)] in the absence of an initial magnetic field.

In the absence of viscosity we can obtain a simple 2-D solution for $k \to \infty$, which gives the fastest growing mode,

$$\omega \to \pm c_{\rm s}k + i\frac{f_\beta v_{\rm A} c_{\rm s}\sin\theta}{2D_B\hat{L}}\left(\frac{v_{\rm A}\hat{L}\sin\theta}{f_\beta c_{\rm s}} \mp 1\right), \quad k \to \infty,\ \nu = 0. \tag{70}$$

The only change from Eq. (43) is that $v_{\rm A}$ is multiplied by $\sin\theta$; the instability is driven by the perpendicular component of the magnetic field. In 2-D there is no upper limit on the magnetic field for growth, so the maximum growth rate given in Eq. (44) and Eq. (46) is achieved for $v_{\rm A}/c_{\rm s} \geq f_\beta/(2\hat{L})$ or equivalently $B_0 \geq f_\beta T_{\rm e}'/(2c_{\rm s})$. When the limit is exceeded the fastest growing mode occurs at decreasing angles to the magnetic field, which will grow a magnetic field component perpendicular to the original field.

IV. FORMATION OF FILAMENTS IN LASER-PLASMAS

We will now consider whether MHD filamentation might explain the formation of filaments in underdense plasma produced by laser–solid interactions. When a laser ablates a solid target, plasma is formed with a density that decays rapidly away from the target surface and with temperature gradients parallel to the target surface due to variations in the laser intensity, generating a magnetic field around the laser spot or intensity spikes within the spot. In addition, laser-energy deposition tends to be localized near the critical surface, creating steep temperature gradients perpendicular to the target surface that could drive instability parallel to the surface. In most cases of interest, there is no applied magnetic field; therefore, we must assume that a large-scale density gradient generates the

initial magnetic field and apply our results to small-scale density perturbations once the initial field has developed, assuming that they evolve much faster than the large-scale field. We must also assume that laser heating maintains an approximately constant electron temperature gradient during the growth time, which is a reasonable assumption. In practice, the development of MHD filaments in plasma produced by laser–solid interactions will be a dynamic, nonlinear process that can only be captured by numerical simulations. We can make estimates, however, to see if this mechanism is worth considering in such detail. For the purposes of estimates, we will assume isothermal electrons ($\gamma_\mathrm{e} = 1$) and ions ($\gamma_\mathrm{i} = 1$) with equal temperatures (T), and $f_\beta \sim 1$.

The laser wavelength in an underdense plasma is much less than the ion collisionless skin depth (δ_i), so gradients in the laser intensity can give $\hat{L}$ $[(L/\delta_\mathrm{i})(1 + 1/Z)]$ less than 1, which will ensure that growth can occur. We can write

$$\delta_\mathrm{i} \approx 42.8 \sqrt{\frac{A}{Z}\frac{n_\mathrm{c}}{n_\mathrm{e}}}\lambda_\mathrm{las}, \tag{71}$$

where n_c is the critical density,

$$n_\mathrm{c} \approx 1.1 \times 10^{27} \left(\frac{\lambda_\mathrm{las}}{1\ \mu\mathrm{m}}\right)^{-2}\ \mathrm{m}^{-3}, \tag{72}$$

and λ_las is the wavelength of the laser. On the other hand, we have found that kinetic effects limit the minimum effective value of L in the self-generated magnetic field to[20]

$$L_\mathrm{min} \sim 3.9a\sqrt{\frac{Z + 0.24}{Z(Z + 4.2)}} \left(\frac{T}{1\ \mathrm{keV}}\right)^2 \left(\frac{n_\mathrm{e}}{10^{27}\ \mathrm{m}^{-3}}\right)^{-1} \left(\frac{\ln\Lambda}{10}\right)^{-1}\ \mu\mathrm{m}, \tag{73}$$

where the multiplier a varies from about 1 to around 2.6, depending on the nature of the heating and cooling. Equation (73) exceeds the laser wavelength for many parameters of interest and gives

$$\hat{L}_\mathrm{min} \sim \frac{0.17a}{\sqrt{A}} \left(\frac{T}{1\ \mathrm{keV}}\right)^2 \left(\frac{n_\mathrm{e}}{10^{27}\ \mathrm{m}^{-3}}\right)^{-1/2} \left(\frac{\ln\Lambda}{10}\right)^{-1}, \tag{74}$$

which will still ensure growth. If the magnetic field becomes high enough to give an electron Hall parameter much greater than one then Eq. (74) will be considerably reduced.

Using Eq. (44), we estimate the maximum possible growth rate of the instability to be

$$\gamma \sim \frac{490}{Z+1}\left(\frac{L}{10\ \mu\text{m}}\right)^{-2}\left(\frac{T}{1\ \text{keV}}\right)^{5/2}\left(\frac{n_\text{e}}{10^{27}\ \text{m}^{-3}}\right)^{-1}\left(\frac{\ln\Lambda}{10}\right)\ \text{ns}^{-1}, \tag{75}$$

where we have used the unmagnetized resistivity; an electron Hall parameter much greater than one would lower the growth rate by a factor of 2. Equation (75) shows that significant growth is possible in a nanosecond and that growth will be faster at lower densities, which agrees with observations.[1] The magnetic field required to achieve the maximum growth rate [Eq. (46)] is

$$B \sim 160\sqrt{\frac{A}{Z+1}}\left(\frac{L}{10\ \mu\text{m}}\right)^{-1}\left(\frac{T}{1\ \text{keV}}\right)^{1/2}\ \text{T}. \tag{76}$$

Magnetic fields of this order of magnitude have been reported in experiments and simulations of laser–solid interactions. For lower magnetic fields, the maximum growth rate will start to fall $\propto B$, so growth over 1 ns could still be significant for a magnetic field of 10 T. For higher magnetic fields, the 2-D result [Eq. (66)] shows us that maximum growth will occur at decreasing angles to the magnetic field.

To estimate the minimum filament width, we need to include viscosity as well as resistivity. The viscous regime is determined by the ratio of viscous velocity diffusion to resistive magnetic diffusion R, which we estimate to be

$$R \sim \left(\frac{620}{A^{1/2}Z^4}+\frac{31}{AZ}\right)\left(\frac{T}{1\ \text{keV}}\right)^{4}\left(\frac{n_\text{e}}{10^{27}\ \text{m}^{-3}}\right)^{-1}\left(\frac{\ln\Lambda}{10}\right)^{-2}, \tag{77}$$

where the first term in brackets is ion viscosity and the second term is electron viscosity, neglecting some small variations in the coefficients at low Z and the effect of electron magnetization.[19] For electron Hall parameters much greater than one, R will be reduced by a factor of 4 because viscosity falls by a factor of 2 and resistivity increases by a factor of 2. It is clear from Eq. (77) that for $Z \leq 3$, ion viscosity dominates and we expect $R > 1$, and that for $Z \geq 4$, electron viscosity dominates and we expect $R < 1$, except for lower densities and higher temperatures where we will always have $R > 1$. We note that the value of R in low-Z plasmas could be lower by a factor of $(T_\text{i}/T_\text{e})^{5/2}$ if the ion temperature is lower than the electron temperature, which does occur in laser-heated plasmas since the laser heats the electrons.

To estimate a minimum wavelength for growth ($2\pi/k_{\max}$), we will use the simple result for $v_\beta = 0$ and $\hat{L} \ll \hat{L}_{\max}$, considering the limits $R \gg 1$, where the result is independent of viscosity, and $R \ll 1$

$$\frac{\lambda_{\min}}{L} \sim 0.11 \frac{Z + 1.23}{2.23} \left(\frac{T}{1\ \text{keV}} \right)^{-2} \left(\frac{n_\text{e}}{10^{27}\ \text{m}^{-3}} \right)^{1/2} \left(\frac{\ln \Lambda}{10} \right), \quad R \gg 1, \tag{78}$$

$$\frac{\lambda_{\min}}{L} \sim 0.26 \sqrt{Z} \sqrt{1 + \frac{20 (A/Z)^{1/2}}{Z^{5/2}}}, \quad R \ll 1, \tag{79}$$

where the Z factor in Eq. (78) comes from a fit to the more involved factor resulting from the expression for unmagnetized resistivity given by Ji–Held.[19] Equations (78) and (79) indicate that the filament width should be proportional to L and increase slowly with Z, but only vary with temperature and density for high viscosity, which typically means at low-Z. Even for the highest values of Z of interest, the smallest filaments will have a wavelength of the order of the temperature gradient scale length.

The Debye length given by $\sqrt{\varepsilon_0 T_\text{e}/(n_\text{e} e)}$, which would determine the minimum filament width in a two-fluid model, is 7.4 nm for our reference values of 1 keV and 10^{27} m^{-3}, so the viscous limit is greater for parameters of interest.

We have established that the MHD filamentation instability could produce fully developed micron-scale filaments in the underdense plasma created by nanosecond laser–solid interactions by considering the maximum possible growth rate and the smallest possible wavelength. To give more detailed estimates, in Fig. 4 we plot the maximum growth rate and the wavelength at which maximum growth occurs from a numerical solution to the full dispersion relation [Eq. (17)] for $L = 10$ μm, $B = 100$ T, temperatures from 50 eV to 10 keV, and electron densities from 10^{25} m^{-3} to 3×10^{27} m^{-3} in fully ionized hydrogen ($Z = 1$, $A = 1$) and carbon ($Z = 6$, $A = 12$) plasmas. We chose hydrogen and carbon because plastics principally composed of these elements are often used in laser–solid experiments, because hydrocarbon contaminants are present on most targets, and because hydrogen has a uniquely high viscosity. The viscosity of helium ($Z = 2$, $A = 4$) is a factor of 23 lower and the viscosity of carbon a factor of 10^3 lower than hydrogen. We do not expect kinetic limitation of the temperature gradient scale length L to be significant for these parameters due to strong magnetization at the lower densities and higher temperatures.[20] For the parameters chosen, viscosity is always significant, but v_β is only significant near the edge of

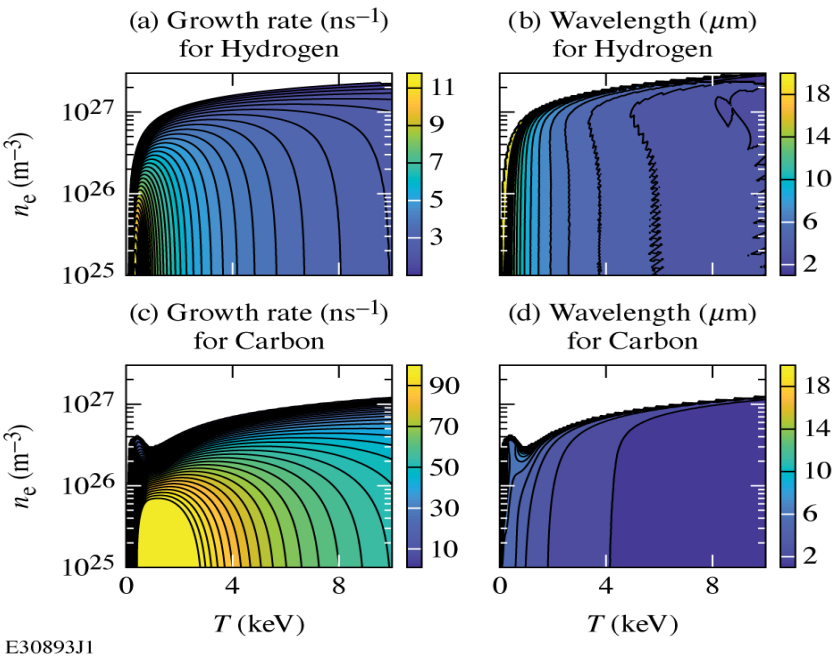

FIG. 4. The maximum growth rate for $L = 10$ μm, $B = 100$ T in (a) hydrogen ($Z = 1$, $A = 1$) and (b) carbon ($Z = 6$, $A = 12$) plasmas as a function of temperature and density, and in (c) and (d) the wavelength at which maximum growth is achieved.

the region of growth due to the electron Hall parameter being too high [Eq. (27)].

In the inviscid case [Eq. (44)], growth would occur for temperatures exceeding 190 eV in hydrogen, 56 eV in carbon, the growth rate would increase rapidly with temperature, decrease with density, and reach higher values in hydrogen than in carbon. In Figs. 4(a) and 4(b) we see that the inviscid threshold temperatures are quite accurate because viscosity is low at these temperatures, but that viscosity leads to a maximum density for growth; growth rates that are weakly dependent on density well below the maximum; a fall in growth rate at high temperature; and significantly slower growth rates in hydrogen than carbon, so much so that we would not expect to see filaments in a hydrogen plasma. The maximum density occurs due to the minimum value of v_A/c_s and the maximum value of $\hat{L}$ introduced by viscosity. The minimum value of v_A/c_s determines the maximum density in hydrogen and in carbon at high temperatures. The maximum value of $\hat{L}$ causes the dip in maximum density

seen in carbon. The maximum density introduced by viscosity improves the agreement with observations, where the filaments seem to be concentrated in low-density plasma.

In the inviscid case, maximum growth occurs at zero wavelength, so a physical result for the fastest growing wavelength can only be obtained with viscosity. The wavelengths for maximum growth seen in Figs. 4(c) and 4(d) depend mainly on temperature well within the region of growth. In carbon, the wavelengths of the fastest growing modes below an electron density $\sim 10^{26}$ m^{-3} and above a temperature of 0.3 keV are practically independent of density and decrease with temperature from about 6 μm at 0.3 keV to 1.3 μm at 10 keV. In hydrogen, similar behaviour to carbon is exhibited above 0.5 keV, but the wavelengths of the fastest growing modes are a factor of roughly 2.4 higher than in carbon. Close to the edge of the region of growth, the wavelengths of the fastest growing modes become much greater and are off the scales used in Figs. 4(c) and 4(d). We note that the wavelength of the fastest growing mode is only indicative of the filament width that might be observed. In practice, the width of the filaments observed will depend on the saturation amplitudes of the modes present, possible filament merging, and the spatial resolution of the measurements. A possible saturation mechanism is perpendicular magnetic field growing above the maximum value, which is larger the lower the wavenumber [Eq. (50)], as illustrated in Fig. 3, so longer wavelengths could dominate observations. The only certain conclusion we can reach on the filament width is that observation of filaments narrower than the minimum width would rule out this instability.

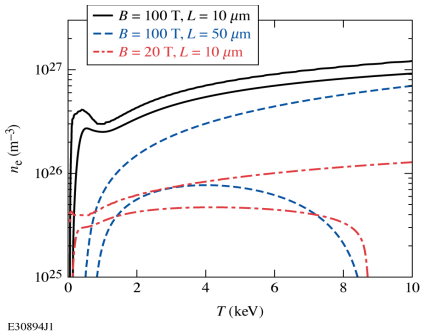

FIG. 5. The 1 ns^{-1} and 20 ns^{-1} growth rate contours in temperature and electron density for varying values of L and B at $Z = 6$, $A/Z = 2$.

The growth rate will fall and the wavelength will increase for longer temperature gradient

scale lengths and lower magnetic fields. Without detailed simulations or measurements, we cannot be certain of the value of the magnetic field and the electron temperature gradient at a given density and temperature. Of particular interest is determining the values at which we would not expect to observe filaments over nanosecond time scales. Figure 5 illustrates the region of instability by plotting the 1 ns^{-1} and 20 ns^{-1} growth rate contours when L is increased by a factor of 5 to 50 μm and B is reduced by a factor of 5 to 20 T. The 1 ns^{-1} contour is close to the edge of the region of growth; 20 ns^{-1} was chosen to be just below the highest growth rate of the $L = 50$ μm case, which had the lowest value at 34 ns^{-1}. The factor of 5 was chosen to give lines that are clearly separated yet still clearly visible on the same plot. Increasing L shrinks the region of growth in both temperature and density, while decreasing B reduces the maximum density. The maximum growth rate well within the region of growth scales as $\sqrt{B}/L$, the square root of the scaling for the inviscid case. To obtain a maximum growth rate of at least 10 ns^{-1} in this region of parameter space should therefore require $L < 140$ μm and $B > 0.53$ T; only at such a low magnetic field very low densities would be required. The factor of 5 increase in L and reduction in B both increased the wavelength of the fastest-growing modes well within the region of growth by a factor of roughly 1.7, indicating an $(L/B)^{1/3}$ scaling for these parameters, which follows the scaling of the characteristic velocity V [Eq. (20)].

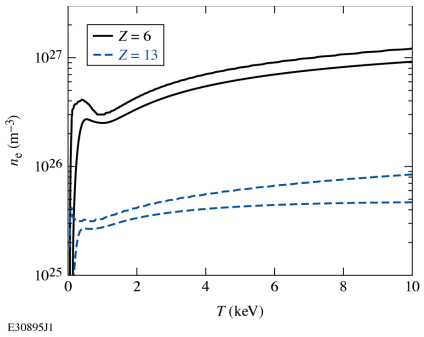

FIG. 6. The 1 ns^{-1} and 20 ns^{-1} growth rate contours in temperature and electron density for $Z = 6$ and $Z = 13$ with $A/Z = 2$, $L = 10$ μm, and $B = 100$ T.

Finally, we consider the effect of further increasing Z by comparing the 1 ns^{-1} and 20 ns^{-1} growth rate contours for $Z = 6$ and $Z = 13$, both with $A/Z = 2$, in Fig. 6. The increase in Z from 6 to 13 increases the ion sound speed by a factor of 1.4 and reduces the

viscosity by a factor of 5.9. The maximum density is reduced, which also occurred when Z was increased from 1 to 6. Well within the region of growth, the growth rates are reduced and the wavelengths are increased by moving from $Z = 6$ to 13, both by a factor of around 1.8, which approaches the inviscid maximum growth rate scaling of $1/(Z+1)$ [Eq. (44)]. At $Z = 1$, growth rates were significantly lower than for both $Z = 6$ and $Z = 13$ due to the high viscosity. We will not consider higher values of Z since it becomes completely unreasonable to consider a fully ionized plasma, even at multi-keV temperatures. Additionally, determining the appropriate values of resistivity and viscosity to find the growth rates and wavelengths in partially ionized, multispecies plasma is complex.

V. APPLICATION TO MHD CODES

The principle application of our results to MHD codes will be in testing the implementation of self-generated magnetic field and the perpendicular electrothermal coefficient. Two-dimensional runs with a fixed out-of-plane electron temperature gradient, isothermal or adiabatic equations of state, and small, initial perturbations can be compared to numerical solutions of Eq. (66). For testing the implementation of the perpendicular electrothermal coefficient, we note that in the (artificial) absence of the magnetic field source term there still exists a driving term due to the electron temperature gradient, with the effective velocity [Eq. (20)] becoming

$$V^3 = -\frac{B_0 T_\mathrm{e}'}{\mu_0 \rho_0}\left(\frac{5}{2} - \frac{3}{2}\gamma_\mathrm{e}\right)\chi_{\mathrm{e}0}\left|\frac{d\beta_{\perp 0}}{d\chi_\mathrm{e}}\right|. \tag{80}$$

Equation (66) could also be used to test the implementation of viscosity.

Our results provide two characteristic velocities V [Eq. (20)] and v_β [Eq. (14)] that must be resolved when self-generated magnetic field and the perpendicular electrothermal coefficient are implemented, respectively. Both of these velocities can significantly exceed the other characteristic velocities of MHD, v_A [Eq. (8)] and c_s [Eq. (19)], when the electron temperature gradient becomes sufficiently steep, requiring significantly lower time steps in MHD codes. The value of v_β can become particularly large over a relatively narrow range of small electron Hall parameters [Sec. II A], which would likely cause an MHD code to stop. In order to avoid excessively large velocities, limiting of the effective temperature gradient may need to be applied to the perpendicular electrothermal term, which has been observed in kinetic simulations for other transport terms and self-generated magnetic field.[20–22] For thermal

transport, however, such temperature gradient or flux limiting is best avoided since this artificially enhances the electron temperature gradient where the limiting occurs and reduces it further down the temperature gradient. An accurate electron temperature gradient is crucial to obtain accurate results for magnetic field generation and transport. Thermal flux limiting has been shown to overestimate the self-generated magnetic field in comparison to kinetic simulations,[21] and lead to failure to converge in resistive MHD by causing resistivity gradients dependent on the grid spacing.[23] No flux limiting can result in electron temperature profiles closer to those from kinetic simulations,[24] although it does allow unphysically high heat fluxes prior to the electron temperature profile relaxing.[23] Ideally, a nonlocal model should be used for the thermal transport when the mean free path is not much less than the temperature gradient scale length.

Our results show that the formation of filaments over nanosecond time scales in laser-produced plasma could be simulated with MHD codes. PIC simulations[12,13] indicate that kinetic effects will be important when the temperature gradient scale length exceeds the ion collisionless skin depth and is smaller than the electron mean free path, which is a regime where the MHD instability is suppressed. However, MHD simulations will need to include viscosity and maintain high spatial resolution, which will still push the limits of current computational capabilities. The fine spatial resolution required in the very underdense plasma effectively rules out a purely Lagrangian simulation, where the cell width will become increasingly large as density decreases. Under-resolved simulations without viscosity can be used to study the dynamic, nonlinear aspects of the problem, but not the expected width of the filaments; our results can be used to determine if the chosen spatial resolution is under or overestimating the growth rates. It should be noted that some MHD codes use artificial resistivity to prevent instabilities on the scale of the grid spacing[25] that would interfere with the development of the instability. The origin of this work were results from inviscid, resistive, 2-D MHD simulations that showed the formation of filaments.[1] Our original simulations used an Eulerian code, without artificial resistivity and without flux limiting.

VI. CONCLUSIONS

We have shown that the equations of MHD can lead to filamentation when self-generated magnetic field and an electron temperature gradient are present. In order to demonstrate

this with a linearized model, we had to assume a fixed, out-of-plane electron temperature gradient while neglecting all dynamics in the direction of the electron temperature gradient, and an initial in-plane magnetic field. In practice, there will be dynamics in the direction of the electron temperature gradient and the initial magnetic field may be self-generated in the plasma, leading to a multidimensional, dynamic, nonlinear problem. The linear model, however, can provide useful insights, despite its limitations.

The 1-D dispersion relation obtained from the linearized MHD equations provides modified magnetoacoustic modes and an additional mode that only occurs in the presence of an electron temperature gradient. The magnetoacoustic mode traveling in the $\nabla T_\mathrm{e} \times \vec{B}_0$ propagates at a reduced velocity due to the electron temperature gradient and can grow exponentially in time. The magnetoacoustic mode traveling in the $-\nabla T_\mathrm{e} \times \vec{B}_0$ propagates at an increased velocity due to the electron temperature gradient and is typically damped. The additional mode travels in the $\nabla T_\mathrm{e} \times \vec{B}_0$ at a velocity less than or equal to the slow magnetoacoustic mode and is also typically damped. The 2-D dispersion relation also provides Alfvén waves and acoustic waves traveling parallel to the magnetic field that are unaffected by the electron temperature gradient.

The key conclusions from the 1-D linearized model [Eq. (17)] are that growth will occur for sufficiently small electron temperature gradient scale lengths determined by the ion collisionless skin depth, and for perpendicular magnetic fields below the advection limited value.[15] The most useful results are Eqs. (45) and (46) to estimate the maximum possible growth rate and Eq. (55) to estimate the maximum possible wavenumber (minimum wavelength). The key conclusion from the 2-D linearized model [Eq. (66)] is that growth can occur at an increasingly acute angle to the magnetic field when it exceeds the maximum value for growth since the instability is driven by the perpendicular component of the magnetic field.

An important conclusion is that both viscosity and resisitivity are required to prevent growth at arbitrarily small spatial scales and to give physical results for the fastest growing modes. Our results show that the ratio of viscous velocity diffusion to resistive magnetic field diffusion is a key dimensionless parameter in MHD, which we have labeled R. Even for $R \ll 1$, viscosity considerably reduces the parameter space where growth occurs, introducing a minimum electron temperature gradient, a maximum wavenumber, and a minimum magnetic field. Viscosity always significantly reduces the maximum growth rate, which without

viscosity would occur at zero wavelength.

We have considered the contribution of the perpendicular electrothermal coefficient to the dispersion relation and have found that it is only significant for a limited range of small electron Hall parameters. In the inviscid case, the perpendicular electrothermal coefficient causes a reduction in magnetic field growth rates of no more than 40% and is negligible for electron Hall parameters much less than 1 or greater than ~ 2 (Fig. 1). With viscosity, the perpendicular electrothermal coefficient also modifies the region of growth, decreasing it for $R < 1$ and increasing it for $R > 1$, but the effect is only significant over a narrow range of very low electron Hall parameters [Eq. (27)]. For typical parameters of interest, the perpendicular electrothermal coefficient can reasonably be neglected when studying filamentation in MHD.

We have found that the MHD filamentation instability could explain observations of filaments in underdense plasma produced by laser–solid interactions.[1–3] In this case, the electron temperature gradient is maintained by laser heating of the plasma, and an initial magnetic field is generated by variations in heating with laser intensity and the fall in electron density away from the solid surface. The dispersion relation [Eq. (17)] indicates growth rates of micron-scale density perturbations robustly above 1 ns^{-1} in underdense plasma for a wide range of relevant temperatures, electron temperature gradient scale lengths, and initial magnetic fields. The only exception is for a hydrogen plasma, where the high ion viscosity leads to low growth rates. In order to investigate the formation of filaments in more detail with an MHD code, viscosity must be included and a very high spatial resolution maintained, which can be determined from our results. In MHD codes without viscosity, the dispersion relation can be used to indicate if the growth rates are being over or underestimated by the choice of spatial resolution. In some MHD codes, growth will be suppressed by artificial resistivity,[25] which is intended to suppress the growth of modes at the grid spacing. When the temperature gradient scale length is too great for the MHD instability to occur, kinetic filamentation modes can still occur.[12,13] The transition between the MHD and kinetic regimes of filamentation or Weibel-like instabilities is something that remains to be fully explored.

The 2-D dispersion relation we have obtained [Eq. (66)] can be used to test the implementation of self-generated magnetic field, the perpendicular electrothermal coefficient, and viscosity in MHD codes.

Finally, the modifications to plasma waves due to an electron temperature gradient could be used to diagnose the temperature gradient in magnetized plasmas.

ACKNOWLEDGMENTS

The information, data, or work presented herein was funded in part by the Advanced Research Projects Agency-Energy (ARPA-E), U.S. Department of Energy, under Award Number DE-AR0001272, by the Department of Energy National Nuclear Security Administration under Award Number DE-NA0003856, the University of Rochester, and the New York State Energy Research and Development Authority. This report was prepared as an account of work sponsored by an agency of the U.S. Government. Neither the U.S. Government nor any agency thereof, nor any of their employees, makes any warranty, express or implied, or assumes any legal liability or responsibility for the accuracy, completeness, or usefulness of any information, apparatus, product, or process disclosed, or represents that its use would not infringe privately owned rights. Reference herein to any specific commercial product, process, or service by trade name, trademark, manufacturer, or otherwise does not necessarily constitute or imply its endorsement, recommendation, or favoring by the U.S. Government or any agency thereof. The views and opinions of authors expressed herein do not necessarily state or reflect those of the U.S. Government or any agency thereof.

VII. AUTHOR DECLARATIONS

A. Conflict of Interest

The author has no conflicts to disclose.

B. Author Contributions

J. R. Davies: Conceptualization (lead); Formal Analysis (lead); Writing - original draft (lead); Writing - review and editing (lead).

VIII. DATA AVAILABILITY

No data was generated.

REFERENCES

[1]J. R. Davies, M. Fajardo, M. Kozlova, T. Mocek, J. Polan and B. Rus, Plasma Phys. Control. Fusion **51**, 035013 (2009).

[2]F. Garcia-Rubio, R. Betti, J. Sanz, and H. Aluie, Phys. Plasmas **29**, 092016 (2022).

[3]G. D. Sutcliffe, P. J. Adrian, J. A. Pearcy, T. M. Johnson, J. Kunimune, B. Pollock, J. D. Moody, N. F. Loureiro, C. K. Li, Observation of electromagnetic filamentary structures produced by the Weibel instability in laser-driven plasmas, acessed 10 August 2023, https://doi.org/10.48550/arXiv.2209.02565

[4]J. J. Bissell, C. P. Ridgers, and R. J. Kingham, Phys. Rev. Lett. **105**, 175001 (2010).

[5]A. R. Bell, R. J. Kingham, H. C. Watkins and J. H. Matthews, Plasma Phys. Control. Fusion **62**, 095026 (2020)

[6]A. B. Hassam, Phys. Fluids **23**, 2493–2497 (1980).

[7]C. K. Li, J. A. Frenje, R. D. Petrasso, F. H. Séguin, P. A. Amendt, O. L. Landen, R. P. J. Town, R. Betti, J. P. Knauer, D. D. Meyerhofer, and J. M. Soures, Phys. Rev. E **80**, 016407 (2009).

[8]E. S. Weibel, Phys. Rev. Lett. **2**, 83 (1959).

[9]F. Califano, F. Pegoraro, and S. V. Bulanov, Phys. Rev. E **56**, 963 (1997).

[10]A. Bret, M.-C. Firpo, and C. Deutsch, Phys. Rev. E **70** 046401 (2004); A. Bret, M.-C. Firpo, and C. Deutsch, Phys. Rev. Lett. **94**, 115002 (2005).

[11]M. E. Dieckmann, G. Sarri, G. C. Murphy, A. Bret, L. Romagnani, I. Kourakis, M. Borghesi, A. Ynnerman, and L. O'C Drury, New Journal of Physics **14**, 023007 (2012).

[12]K. M. Schoeffler, N. F. Loureiro, R. A. Fonseca, and L. O. Silva, Phys. Rev. Lett. **112**, 175001 (2014)

[13]K. M. Schoeffler, and L. O. Silva, Phys. Rev. Research **2**, 033233 (2020).

[14]T. Silva, K. Schoeffler, J. Vieira, M. Hoshino, R. A. Fonseca, and L. O. Silva, Phys. Rev. Research **2**, 023080 (2020); Y. Z. Zhou, C. Y. Zheng, Z. J. Liu, and L. H. Cao, Plasma Phys. Control. Fusion **64**, 045009 (2022).

[15]M. G. Haines, Phys. Rev. Lett. **78**, 254 (1997).

[16]J. D. Sadler, C. A. Walsh, and H. Li, Phys. Rev. Lett. **126**, 075001 (2020). Fits given in the online supplementary material.

[17]S. I. Braginskii, in *Reviews of Plasma Physics*, edited by M. A. Leontovich (Consultants Bureau, New York, 1965), Vol. 1, p. 205.

[18]E. M. Epperlein, and M. G. Haines, Phys. Fluids **29**, 1029 (1986).

[19]J.-Y. Ji, and E. D. Held, Phys. Plasmas **20**, 042114 (2013).

[20]J. R. Davies, Phys. Plasmas **30**, 072701 (2023).

[21]C. P. Ridgers, C. Arran, J. J. Bissell, and R. J. Kingham, Phil. Trans. R. Soc. A **379**, 20200017 (2020).

[22]M. Sherlock, and J. J. Bissell, Phys. Rev. Lett. **124**, 055001 (2020).

[23]J. R. Davies, R. Betti, P.-Y. Chang, and G. Fiksel, Phys. Plasmas **22**, 112703 (2015).

[24]J. P. Brodrick, M. Sherlock, W. A. Farmer, A. S. Joglekar, R. Barrois, J. Wengraf, J. J. Bissell, R. J. Kingham, D. Del Sorbo, M. P. Read, and C. P. Ridgers, Plasma Phys. Control. Fusion **60**, 084009 (2018).

[25]T. D. Arber, A. W. Longbottom, C. L. Gerrard, and A. M. Milne, J. Comput. Phys. **171**, 151 (2001); S. Kawai, J. Comput. Phys. **251**, 292 (2013).